Radio-over-fiber DSB-to-SSB conversion using semiconductor lasers at stable locking dynamics

Kun-Lin Hsieh,[1] **Yu-Han Hung,**[1] **Sheng-Kwang Hwang,**[1,2,*] **and Chien-Chung Lin**[3]

[1]*Department of Photonics, National Cheng Kung University, Tainan, Taiwan*
[2]*Advanced Optoelectronic Technology Center, National Cheng Kung University, Tainan, Taiwan*
[3]*Institute of Photonic System, National Chiao Tung University, Tainan, Taiwan*
[*]*skhwang@mail.ncku.edu.tw*

Abstract: In radio-over-fiber systems, optical single-sideband (SSB) modulation signals are preferred to optical double-sideband (DSB) modulation signals for fiber distribution in order to mitigate the microwave power fading effect. However, typically adopted modulation schemes generate DSB signals, making DSB-to-SSB conversion necessary before or after fiber distribution. This study investigates a semiconductor laser at stable locking dynamics for such conversion. The conversion relies solely on the nonlinear dynamical interaction between an input DSB signal and the laser. Only a typical semiconductor laser is therefore required as the key conversion unit, and no pump or probe signal is necessary. The conversion can be achieved for a broad tunable range of microwave frequency up to at least 60 GHz. In addition, the conversion can be carried out even when the microwave frequency, the power of the input DSB signal, or the frequency of the input DSB signal fluctuates over a wide range, leading to high adaptability and stability of the conversion system. After conversion, while the microwave phase quality, such as linewidth and phase noise, is mainly preserved, a bit-error ratio down to 10^{-9} is achieved for a data rate up to at least 8 Gb/s with a detection sensitivity improvement of more than 1.5 dB.

OCIS codes: (140.5960) Semiconductor lasers; (140.3520) Lasers, injection-locked; (060.4510) Optical communications; (060.5625) Radio frequency photonics; (350.4010) Microwaves; (070.4340) Nonlinear optical signal processing.

References and links

1. C. Lim, A. Nirmalathas, M. Bakaul, P. Gamage, K. L. Lee, Y. Yang, D. Novak, and R. Waterhouse, "Fiber-wireless networks and subsystem technologies," J. Lightwave Technol. **28,** 390–405 (2010).
2. C. Liu, J. Wang, L. Cheng, M. Zhu, and G. K. Chang, "Key microwave-photonics technologies for next-generation cloud-based radio access networks," J. Lightwave Technol. **32,** 3452–3460 (2014).
3. J. Beas, G. Castanon, I. Aldaya, A. Aragon-Zavala, and G. Campuzano, "Millimeter-wave frequency radio over fiber systems: A survey," IEEE Commun. Surveys Tuts. **15,** 1593–1619 (2013).
4. G. J. Meslener, "Chromatic dispersion induced distortion of modulated monochromatic light employing direct detection," IEEE J. Quantum Electron. **20,** 1208–1216 (1984).
5. U. Gliese, S. Norskov, and T. N. Nielsen, "Chromatic dispersion in fiber-optic microwave and millimeter-wave links," IEEE Trans. Microwave Theory Tech. **44,** 1716–1724 (1996).

#261981 Received 28 Mar 2016; revised 23 Apr 2016; accepted 23 Apr 2016; published 27 Apr 2016

6. G. H. Smith, D. Novak, and Z. Ahmed, "Overcoming chromatic-dispersion effects in fiber-wireless systems incorporating external modulators," IEEE Trans. Microwave Theory Tech. **45,** 1410–1415 (1997).
7. X. S. Yao, "Brillouin selective sideband amplification of microwave photonic signals," IEEE Photon. Technol. Lett. **10,** 138–140 (1998).
8. A. Loayssa, D. Benito, and M. J. Garde, "Optical carrier-suppression technique with a Brillouin-erbium fiber laser," Opt. Lett. **25,** 197–199 (2000).
9. A. Kaszubowska, P. Anandarajah, and L.P. Barry, "Multifunctional operation of a fiber Bragg grating in a WDM/SCM radio over fiber distribution system," IEEE Photon. Technol. Lett. **16,** 605–607 (2004).
10. Y. Shen, X. Zhang, and K. Chen, "Optical single sideband modulation of 11-GHz RoF system using stimulated Brillouin scattering," IEEE Photon. Technol. Lett. **17,** 1277–1279 (2005).
11. S. R. Blais and J. Yao, "Optical single sideband modulation using an ultranarrow dual-transmission-band fiber Bragg grating," IEEE Photon. Technol. Lett. **18,** 2230–2232 (2006).
12. W. Li, N. H. Zhu, L. X. Wang, X. Q. Qi, and L. Xie, "Tunable carrier generation and broadband data conversion for RoF system based on stimulated Brillouin scattering," IEEE Trans. Microw. Theory Tech. **59,** 2350–2356 (2011).
13. Y. H. Hung, C. H. Chu, and S. K. Hwang, "Optical double-sideband modulation to single-sideband modulation conversion using period-one nonlinear dynamics of semiconductor lasers for radio-over-fiber links," Opt. Lett. **38,** 1482–1484 (2013).
14. Y. H. Hung and S. K. Hwang, "Photonic microwave amplification for radio-over-fiber links using period-one nonlinear dynamics of semiconductor lasers," Opt. Lett. **38,** 3355–3358 (2013).
15. T. B. Simpson, J. M. Liu, K. F. Huang, and K. Tai, "Nonlinear dynamics induced by external optical injection in semiconductor lasers," Quantum Semiclass. Opt. **9,** 765–784 (1997).
16. V. Annovazzi Lodi, A. Scire, M. Sorel, and S. Donati, "Dynamical Behavior and Locking of Semiconductor Laser Subjected to Injection", IEEE J. of Quantum Electron. **34,** 2350–2356 (1998).
17. S. K. Hwang and J. M. Liu, "Dynamical characteristics of an optically injected semiconductor laser," Opt. Commun. **183,** 195–205 (2000).
18. S. K. Hwang, J. M. Liu, and J. K. White, "Characteristics of period-one oscillations in semiconductor lasers subject to optical injection," IEEE J. Sel. Top. Quantum Electron. **10,** 974–981 (2004).
19. S. Wieczorek, B. Krauskopf, T.B. Simpson, and D. Lenstra, "The dynamical complexity of optically injected semiconductor lasers," Physics Reports **416,** 1–128 (2005).
20. S. C. Chan, "Analysis of an optically injected semiconductor laser for microwave generation," IEEE J. Quantum Electron. **46,** 421–428 (2010).
21. T. B. Simpson, J. M. Liu, and A. Gavrielides, "Small-signal analysis of modulation characteristics in a semiconductor laser subject to strong optical injection," IEEE J. Quantum Electron. **32,** 1456–1468 (1996).
22. A. Murakami, K. Kawashima, and K. Atsuki, "Cavity resonance shift and bandwidth enhancement in semiconductor lasers with strong light injection," IEEE J. Quantum Electron. **39,** 1196–1204 (2003).
23. S. K. Hwang, S. C. Chan, S. C. Hsieh, and C. Y. Li, "Photonic microwave generation and transmission using direct modulation of stably injection-locked semiconductor lasers," Opt. Commun. **284,** 3581–3589 (2011).
24. T. B. Simpson, J. M. Liu, and A. Gavrielides, "Bandwidth enhancement and broadband noise reduction in injection-locked semiconductor lasers," IEEE Photon. Technol. Lett. **7,** 709–711 (1995).
25. T. B. Simpson and J. M. Liu, "Enhanced modulation bandwidth in injection-locked semiconductor lasers," IEEE Photon. Technol. Lett. **9,** 1322-1324 (1997).
26. Y. Okajima, S.K. Hwang, and J.M. Liu, "Experimental observation of chirp reduction in bandwidth-enhanced semiconductor lasers subject to strong optical injection," Opt. Commun. **219,** 357–364 (2003).
27. S. K. Hwang, J. M. Liu, and J. K. White, "35-GHz intrinsic bandwidth for direct modulation in 1.3-μm semiconductor lasers subject to strong injection locking," IEEE Photon. Technol. Lett. **16,** 972–974 (2004).
28. E. K. Lau, X. Zhao, H. K. Sung, D. Parekh, C. J. Chang-Hasnain, and M. Wu, "Strong optical injection-locked semiconductor lasers demonstrating $>$ 100-GHz resonance frequencies and 80-GHz intrinsic bandwidths," Opt. Express **16,** 6609–6618 (2008).
29. K. L. Hsieh, Y. H. Hung, and S. K. Hwang, "Optical DSB-to-SSB conversion for radio-over-fiber links utilizing semiconductor lasers at stable locking dynamics," in Proceedings of 2014 OptoElectronics and Communication Conference and Australian Conference on Optical Fibre Technology (IEEE, 2014), pp. 132–134.
30. J. Li, J. Q. Liu, and D. P. Taylor, "Optical communication using subcarrier PSK intensity modulation through atmospheric turbulence channels," IEEE Trans. Commun. **55,** 1598–1606 (2007).
31. I. S. Ansari, F. Yilmaz, and M.-S. Alouini, "On the performance of hybrid RF and RF/FSO dual-hop transmission systems," in Proceedings of 2013 2nd International Workshop on Optical Wireless Communicaitons (IEEE, 2013), pp. 45–49.
32. K. Vahala and A. Yariv, "Semiclassical theory of noise in semiconductor lasers - part II," IEEE J. Quantum Electron. **19,** 1102–1109 (1983).
33. M. T. van Exter, W. A. Hamel, J. P. Woerdman, and B. R. P. Zeijlmans, "Spectral signatures of relaxation oscillations in semiconductor lasers," IEEE J. Quantum Electron. **28,** 1470–1478 (1992).
34. R. Adler, "A study of locking phenomena in oscillators," Proc. IRE and Waves and Electrons **34,** 351–357 (1946).

#261981 Received 28 Mar 2016; revised 23 Apr 2016; accepted 23 Apr 2016; published 27 Apr 2016

35. S. Donati and S. K. Hwang, "Chaos and high-level dynamics in coupled lasers and their applications," Progress in Quantum Electron. **36,** 293–341 (2012).

1. Introduction

Radio-over-fiber has attracted great attention due to the strong demand in distributing microwave subcarriers over long distances through fibers for broadband wireless access networks [1, 2]. External or direct modulation of semiconductor lasers is the simplest scheme to superimpose microwave subcarriers onto optical carriers for such radio-over-fiber systems [3]. Owing to the inherent nature of either modulation scheme, an optical double-sideband (DSB) modulation signal is typically generated, in which the power of the two modulation sidebands around the optical carrier is the same. Such a DSB feature leads to severe microwave power fading over fiber distribution of the optical signal [4, 5], which results from a walk-off in the relative phases of the two modulation sidebands to the optical carrier due to fiber chromatic dispersion. To mitigate the fading effect, it is preferable that only one modulation sideband exists, or, more loosely speaking, one modulation sideband is much stronger than the other, leading to a feature of optical single-sideband (SSB) modulation. Therefore, it becomes necessary to perform DSB-to-SSB conversion for either modulation scheme before or after fiber distribution. Various different conversion approaches and systems have been proposed accordingly [6–14].

For example, Smith *et al.* suggested a dual-electrode Mach-Zehnder modulator with a precise control of the relative phase between the two microwave signals applied to the two electrodes, respectively [6]. This, however, limits the applicability of the approach to the external modulation scheme only. In addition, an electronic microwave phase shifter and an electronic microwave power divider are required. This makes the approach increasingly difficult or expensive to implement for increasingly high microwave subcarrier frequency owing to the electronic bandwidth limitation. Yao proposed to apply the stimulated Brillouin scattering in an optical fiber to considerably amplify one modulation sideband of an input DSB signal through the Brillouin gain [7]. Because of the limited gain bandwidth, a precise frequency control of an optical pump is necessary and the rate of the data carried by a microwave subcarrier is restricted to around 10 Mb/s. The system is therefore required to be highly stable and limited to applications at low data rates only. Moreover, a long fiber, on the order of 10 km, and a strong optical pump, on the order of 10 mW, are required, making the system bulky and power consuming. Kaszubowska *et al.* suggested a fiber Bragg grating to suppress one modulation sideband of an input DSB signal by positioning one edge of its passband close to the optical carrier frequency [9]. An optical amplifier is needed to compensate for the significant optical power loss after conversion, making the approach power consuming. In addition, a fiber Bragg grating of a different center frequency or a different passband width is necessary for a radio-over-fiber system adopting a different optical carrier frequency or a different microwave subcarrier frequency, respectively. This severely restricts the range of either frequency the approach can be applied to once a fiber Bragg grating is given. Hung *et al.* proposed to use the period-one nonlinear dynamics in a semiconductor laser by taking advantage of the significant intensity-asymmetry between the two oscillation sidebands of the dynamics [13]. Frequency locking is required between the modulation sidebands of an input DSB signal and the oscillation sidebands of the dynamics. This limits the extent of converter adaptability and stability when operating conditions fluctuate because of possible ambience variations or different system requirements.

In this study, an approach based on stable locking dynamics of a semiconductor laser is proposed for DSB-to-SSB conversion. The stable locking dynamics can be excited when the laser is subject to continuous-wave (CW) optical injection within the range bounded by a Hopf bifurcation and a saddle-node bifurcation [15–20]. On one hand, the optical injection imposes the injected laser to follow its optical phase and therefore to oscillate at the injection frequency

#261981 Received 28 Mar 2016; revised 23 Apr 2016; accepted 23 Apr 2016; published 27 Apr 2016

instead. On the other hand, the optical injection red-shifts the cavity resonance of the injected laser through the antiguidance effect and therefore radically modifies the relaxation resonance features [20–23]. The two relaxation resonance sidebands substantially shift away from the injected laser oscillation, resulting in a considerable enhancement of the relaxation resonance frequency [24–28]. More interestingly, the lower relaxation resonance sideband highly dominates the upper one, suggesting that the resonance enhancement is significantly stronger at frequencies negatively offset from the injected laser oscillation [21, 23]. The DSB-to-SSB conversion can therefore be achieved by considerably amplifying the lower modulation sideband of an input DSB signal as opposed to the upper one through such a significant difference in the resonance enhancement. The conversion can be carried out no matter how the input DSB signal is generated to begin with, such as external or direct modulation of a laser. Only a typical semiconductor laser is required as the key conversion unit, and no pump or probe signal is necessary. No frequency locking is required as in the period-one dynamics approach, which highly improves the extent of converter adaptability and stability when operating conditions fluctuate. The conversion can be achieved for a significantly broad tunable range of microwave subcarrier frequency up to at least 60 GHz by simply adjusting the frequency and power of the input DSB signal relative to those of the injected laser. Owing to the wide bandwidth of the resonance enhancement, the rate of the data carried by a microwave subcarrier can be considerably high, up to at least 8 Gb/s. Note that a proof-of-concept of the proposed conversion approach has been demonstrated in [29] without addressing the various key performance characteristics indicated above. Therefore, this study provides valuable and comprehensive information to take the best advantages of the proposed conversion approach for practical applications. Also note that radio-over-free-space has recently attracted much research interest for free-space optical communications owing to its promising capability to alleviate signal scintillation introduced by atmospheric turbulence [30, 31]. The proposed conversion approach can be used for such an application to mitigate possible microwave power fading due to chromatic dispersion and to improve detection sensitivity and thus transmission distance. Following this introduction, an experimental setup is presented in Section 2. Results and analyses are reported in Section 3. Finally, a discussion and a conclusion are made in Section 4.

2. Experimental setup

A schematic of the experimental apparatus used for this study is presented in Fig. 1. The proposed DSB-to-SSB conversion system consists of a typical single-mode distributed-feedback semiconductor laser (Furukawa FRL15DCW5-A81), LD2. Under a bias current of 30 mA and a stabilized temperature of 23^{o} C, the free-running LD2 oscillates at 193.411 THz with an optical power of 3.8 mW measured at its fiber-pigtail output and with a relaxation resonance frequency of 8 GHz. An input optical carrier is generated by another single-mode distributed-feedback semiconductor laser of the same model, LD1, and is directed toward LD2 through a circulator. To excite the stable locking dynamics, the frequency of the input optical carrier is detuned by f_{i} from the free-running frequency of LD2 through adjusting either the temperature or the bias current of LD1. In addition, the power of the input optical carrier is varied using an Erbium-doped fiber amplifier and a variable optical attenuator, and is measured at the output port of the circulator connected to LD2. Note that the fiber amplifier is not required if the power of the input optical carrier is adequately high to begin with for the operation of the proposed conversion system. To indicate the injection strength received by LD2, an injection ratio ξ_{i}, defined as the square root of the power ratio between the input optical carrier and the free-running LD2, is used in this study. A polarization controller aligns the polarization of the input optical carrier with that of LD2 to maximize the injection efficiency. A microwave subcarrier at a frequency of f_{m} is first generated by a microwave source (Agilent E8257D) and next superimposed on

#261981 Received 28 Mar 2016; revised 23 Apr 2016; accepted 23 Apr 2016; published 27 Apr 2016

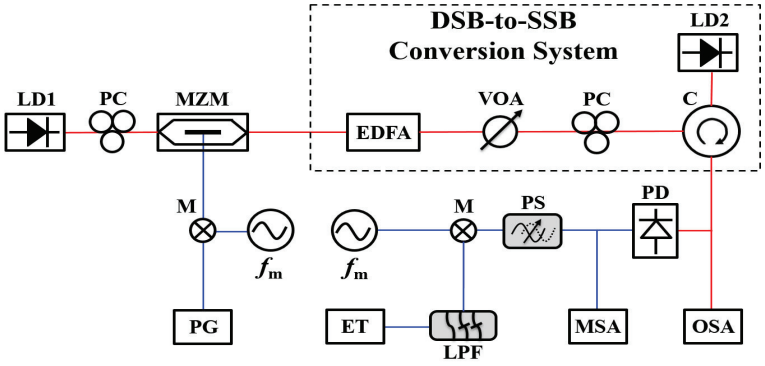

Fig. 1. Schematic of the experimental apparatus. LD1, laser diode 1; PC, polarization controller; MZM, Mach-Zehnder modulator; M, mixer; PG, pattern generator; EDFA, Erbium-doped fiber amplifier; VOA, variable optical attenuator; C, circulator; LD2, laser diode 2; OSA, optical spectrum analyzer; PD, photodiode; MSA, microwave spectrum analyzer; PS, phase shifter; LPF, low-pass filter; ET, error tester.

the input optical carrier through a Mach-Zehnder modulator (EOspace AX-AV5-40) to form an optical DSB signal. Data in a format of binary phase-shift keying from a pattern generator (Anritsu MP2101A) are encoded onto the microwave subcarrier through an electronic microwave mixer. The output of LD2 is sent to an optical spectrum analyzer (Advantest Q8384) and a 50-GHz photodiode (u2t Photonics XPDV2120R). The photodetected signal is monitored by a microwave spectrum analyzer (Agilent N9030A PXA). For the bit-error ratio (BER) analysis, the photodetected signal is first downconverted to the baseband by mixing it with a local microwave oscillator at f_m and is next sent through a low-pass filter before entering an error tester (Anritsu MP2101A).

3. Results and analyses

3.1. Operating principle

Without any external perturbation, LD2 oscillates at the free-running cavity resonance, shown as the black curve in Fig. 2(a). Theoretically, two relaxation resonance sidebands of similar power, which result from the interaction between optical fields and charge carreirs, would emerge equally and oppositely away from the laser oscillation [32, 33]. However, they cannot be experimentally observed due to the limited frequency resolution and detection sensitivity of the optical spectrum analyzer used in this study. The frequency offset between the relaxation resonance sidebands and the laser oscillation is commonly adopted to approximate the relaxation resonance frequency of a laser [21, 33] and is denoted as f_r for the same purpose in this study. The power similarity between the relaxation resonance sidebands implies a similar level of the resonance enhancement at frequencies either negatively or positively offset from the laser oscillation. These characteristics can be radically modified through the introduction of external optical injection within the range bounded by a Hopf bifurcation and a saddle-node bifurcation.

When an input optical carrier without microwave modulation, shown as the blue curve in Fig. 2(a), is injected into LD2 at (ξ_i, f_i) = (1.33, 15.53 GHz), a stable locking dynamical state is excited, shown as the green curve in Fig. 2(a). Owing to the injection pulling effect [34, 35], the input optical carrier imposes LD2 to follow its optical phase and therefore to oscillate at the offset frequency of 15.53 GHz, i.e., at the input optical carrier frequency. In addition, the introduction of the input optical carrier lowers down the optical gain level required for the in-

#261981 Received 28 Mar 2016; revised 23 Apr 2016; accepted 23 Apr 2016; published 27 Apr 2016

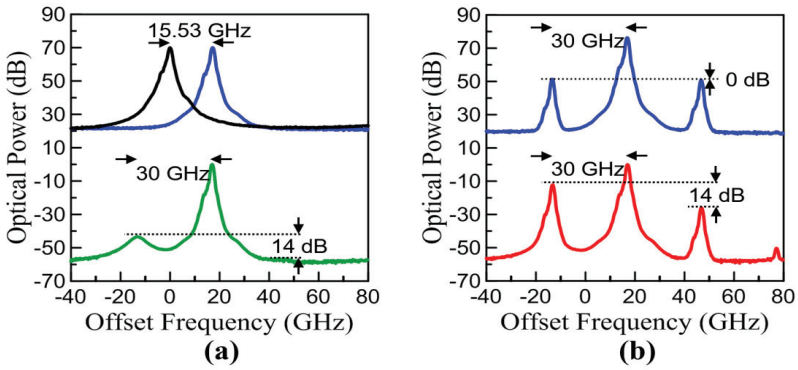

Fig. 2. Optical spectra of (a) free-running output (black curve), CW input (blue curve), and stable locking output (green curve), and (b) DSB input (blue curve) and SSB output (red curve). For visibility, the curves are up- or down-shifted with respect to each other. The x-axes are relative to the free-running frequency of LD2. Inputs are kept at (ξ_i, f_i) = (1.33, 15.53 GHz).

jected LD2, which in turns red-shifts the cavity resonance of LD2 through the antiguidance effect [21–23]. As a result, the two relaxation resonance sidebands shift considerably away from the injected LD2 oscillation, leading to a considerable enhancement of f_r from 8 GHz to 30 GHz. This modified characteristic is beneficial to the proposed conversion approach for high-frequency microwave applications. Moreover, because of the red-shifted cavity resonance, the lower relaxation resonance sideband is resonantly enhanced as opposed to the upper one, resulting in its visible appearance in the spectrum and its dominance over the upper one, about 14 dB higher. This suggests that the resonance enhancement is significantly stronger at frequencies negatively offset from the injected LD2 oscillation.

By taking advantage of such a significant difference in the resonance enhancement, the DSB-to-SSB conversion can be carried out by considerably amplifying the lower modulation sideband of an input DSB signal, as demonstrated in Fig. 2(b). The input optical carrier is now microwave-modulated at $f_m = f_r = 30$ GHz, shown as the blue curve in Fig. 2(b), which generates an input DSB signal with an optical carrier 25-dB stronger than both modulation sidebands, corresponding to an optical modulation depth of 11%. At the same (ξ_i, f_i) = (1.33, 15.53 GHz) considered in Fig. 2(a), an output optical signal with a SSB feature can be obtained, shown as the red curve in Fig. 2(b). While the upper modulation sideband is slightly reduced by about 1 dB, the lower one is substantially enhanced by about 13 dB, leading to a sideband rejection ratio, SRR, of about 14 dB. Note that, in this study, the SRR value of an output optical signal is defined as the relative strength of its lower modulation sideband to the upper one in order to quantify the extent of its SSB feature after conversion. Comparing Fig. 2(b) with Fig. 2(a) suggests that the extent of the SSB feature of the output optical signal is indeed strongly determined by the difference in the resonance enhancement of the stable locking dynamical state between negatively and positively offset frequencies from the injected LD2 oscillation. As will be demonstrated in Fig. 9, such a SRR value is adequately high to considerably mitigate the microwave power fluctuation when the output SSB signal is distributed over fibers. Note that even though external modulation of a semiconductor laser is used to generate input DSB signals in this study, the proposed conversion approach works no matter how input DSB signals are generated to begin with.

#261981 Received 28 Mar 2016; revised 23 Apr 2016; accepted 23 Apr 2016; published 27 Apr 2016

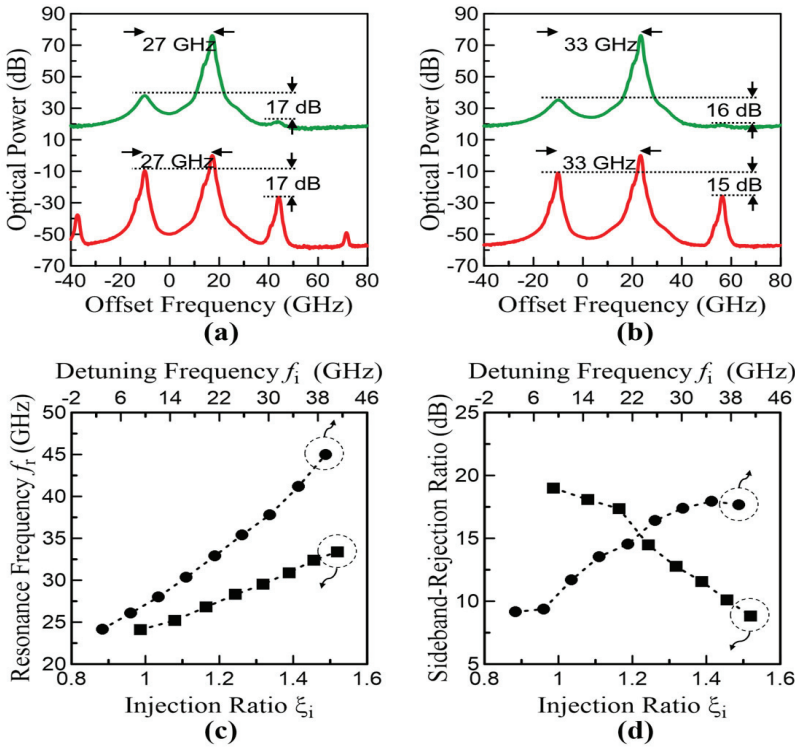

Fig. 3. (a) Optical spectra of the stable locking output (green curve) at (ξ_i, f_i) = (1.17, 15.53 GHz) and the SSB output (red curve) at (ξ_i, f_i, f_m) = (1.17, 15.53 GHz, 27 GHz). (b) Optical Spectra of the stable locking output (green curve) at (ξ_i, f_i) = (1.33, 21.8 GHz) and the SSB output (red curve) at (ξ_i, f_i, f_m) = (1.33, 21.8 GHz, 33 GHz). (c) Relaxation resonance frequency f_r and (d) sideband rejection ratio, SRR, of the stable locking output in terms of ξ_i at $f_i = 15.53$ GHz and in terms of f_i at $\xi_i = 1.33$. In (a) and (b), the curves are up- or down-shifted with respect to each other for visibility, and the x-axes are relative to the free-running frequency of LD2.

3.2. Conversion tunability

Various stable locking dynamical states similar to the one shown in Fig. 2(a) can be excited over a wide range of ξ_i and f_i. For example, as Fig. 3(a) shows, if ξ_i is adjusted from 1.33 to 1.17 while keeping $f_i = 15.53$ GHz, the CW-injected LD2 exhibits a similar stable locking feature yet with $f_r = 27$ GHz and SRR = 17 dB. Note that, in this study, the SRR value of a stable locking dynamical state is defined as the relative strength of its lower relaxation resonance sideband to the upper one in order to quantify the difference of its resonance enhancement between negatively and positively offset frequencies from the injected laser oscillation. On the other hand, as Fig. 3(b) shows, if f_i changes from 15.53 to 21.8 GHz while fixing $\xi_i = 1.33$, the CW-injected LD2 also exhibits a similar stable locking feature but with $f_r = 33$ GHz and SRR = 16 dB. The dependence of f_r and SRR on the injection condition for the CW-injected LD2 at the stable locking dynamics are presented in Figs. 3(c) and 3(d), respectively. In general, f_r increases monotonically with increasing ξ_i or f_i, giving rise to a broadly and continuously tunable f_r up to at least 45 GHz for the operating conditions under study. A higher f_r, such as 100 GHz, can be achieved if ξ_i or f_i can be further increased within the range of the stable locking dynamics, or if a higher free-running f_r is given to begin with by using a higher bias

#261981 Received 28 Mar 2016; revised 23 Apr 2016; accepted 23 Apr 2016; published 27 Apr 2016

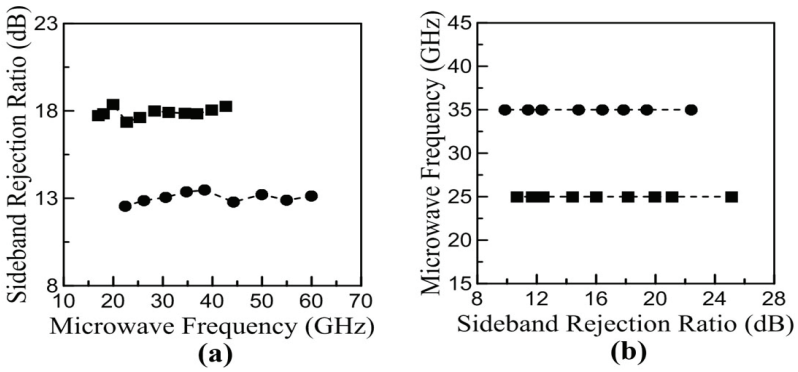

Fig. 4. (a) Tunability in microwave subcarrier frequency for two representative SRR values. (b) Tunability in SRR for two representative microwave subcarrier frequencies.

level of the same laser or a different laser of a higher speed. On the other hand, SRR increases monotonically with decreasing ξ_i or increasing f_i, where SRR of more than 10 dB can be achieved.

By taking advantage of the feasibility in exciting various stable locking dynamical states of different f_r and SRR, an input DSB signal at a specific microwave subcarrier frequency, $f_m = f_r$, can be converted to an output SSB signal with a specific SRR value by simply adjusting ξ_i or/and f_i. For example, for an input DSB signal at $f_m = 27$ GHz, an output SSB signal with SRR = 17 dB can be obtained at (ξ_i, f_i) = (1.17, 15.53 GHz), shown as the red curve in Fig. 3(a). For an input DSB signal at $f_m = 33$ GHz, an output SSB signal with SRR = 15 dB can be obtained at (ξ_i, f_i) = (1.33, 21.8 GHz), shown as the red curve in Fig. 3(b). Hence, by properly manipulating (ξ_i, f_i), an output SSB signal with a specific SRR value can be achieved for a broad range of microwave subcarrier frequency, as shown in Fig. 4(a). On the other hand, an output SSB signal with a wide range of SRR can be obtained for a specific microwave subcarrier frequency, as presented in Fig. 4(b). These tunable characteristics of the proposed conversion system provide a radio-over-fiber system with capability to dynamically reconfigure itself if a different operating condition in the microwave subcarrier frequency or the SSB feature is required.

3.3. System adaptability and stability

For a fixed injection condition (ξ_i, f_i) where f_r is constant, the proposed conversion approach works even when f_m varies around f_r. As Fig. 5(a) presents, at the same (ξ_i, f_i) = (1.33, 15.53 GHz) considered in Fig. 2 where $f_r = 30$ GHz, an input DSB signal at $f_m = 25$ GHz can be converted to an output SSB signal with SRR = 14 dB. This demonstrates that the system can be self-adapted to certain adjustments in f_m, which may result from possible fluctuations in the operating condition or different requirements in different radio-over-fiber systems, without the need to change (ξ_i, f_i). Different from the period-one dynamics approach [13], the modulation sidebands of an input DSB signal do not need to lock, respectively, the relaxation resonance sidebands of a stable locking dynamical state for the proposed approach to achieve the conversion when $f_m \neq f_r$. This characteristic further enables the conversion of an input DSB signal at f_m very far from f_r. For example, as demonstrated in Fig. 5(b) where $f_m = 20$ GHz, an output SSB signal with SRR = 11 dB is obtained at the same (ξ_i, f_i) = (1.33, 15.53 GHz) considered in Fig. 2 where $f_r = 30$ GHz. As noted in Figs. 5(a) and 5(b), the power difference between the two modulation sidebands after conversion depends on f_m. This is more clearly

#261981 Received 28 Mar 2016; revised 23 Apr 2016; accepted 23 Apr 2016; published 27 Apr 2016

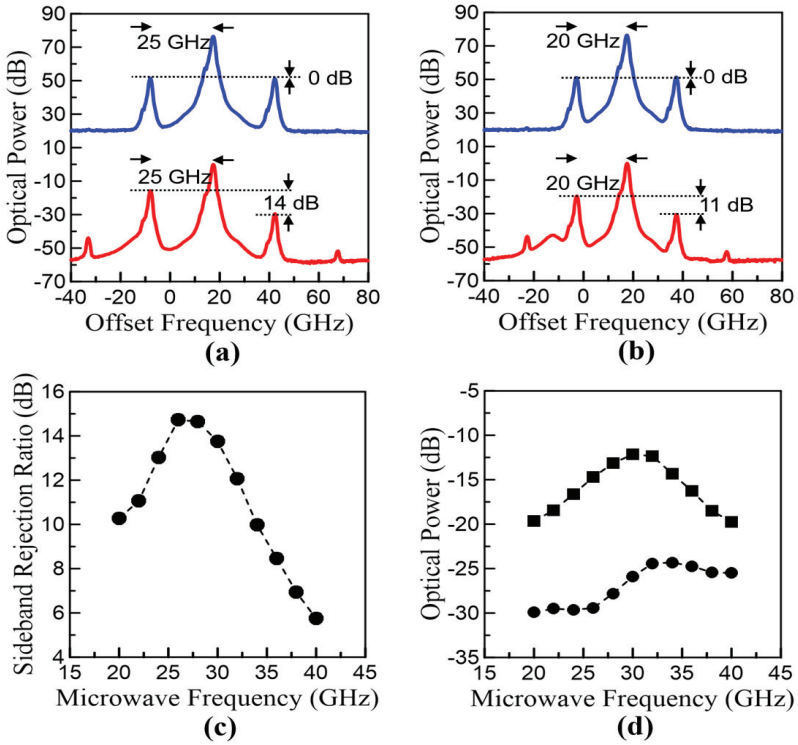

Fig. 5. Optical spectra of DSB inputs (blue curves) and SSB outputs (red curves) at (ξ_i, f_i) = (1.33, 15.53 GHz) for (a) $f_m = 25$ GHz and (b) $f_m = 20$ GHz, respectively. For visibility, the curves are up- or down-shifted with respect to each other. The x-axes are relative to the free-running frequency of LD2. (c) Sideband rejection ratio and (d) optical power of the lower (squares) and upper (circles) modulation sidebands in terms of f_m at (ξ_i, f_i) = (1.33, 15.53 GHz).

demonstrated in Fig. 5(c), where the SRR value reaches its maximum at around $f_m = 27$ GHz, which is 3 GHz below f_r, and decreases monotonically as f_m deviates from 27 GHz. Such a dependence results from the different level of the resonance enhancement as a function of f_m for each modulation sideband, as Fig. 5(d) presents. The increase of SRR is attributed to the fact that the power of the lower modulation sideband enhances significantly before $f_m = 30$ GHz while that of the upper one remains mostly unchanged before $f_m = 27$ GHz. The decrease of SRR, on the other hand, results from the fact that the power of the lower modulation sideband reduces considerably after $f_m = 30$ GHz while that of the upper one enhances moderately after $f_m = 27$ GHz. If SRR = 10 dB, for example, is the minimum requirement for an output SSB signal in a radio-over-fiber system to mitigate the microwave power fading effect to an acceptable level, Fig. 5(c) demonstrates that the proposed conversion approach works well for (ξ_i, f_i) = (1.33, 15.53 GHz) even when f_m varies between 20 and 34 GHz. This system adaptability to f_m adjustment ensures a functioning operation of the proposed conversion system over a considerably broad range of variation in the microwave subcarrier frequency without the need to adjust the injection level and frequency.

For a fixed microwave subcarrier frequency f_m, the proposed conversion approach also works even when ξ_i or f_i fluctuates, i.e., even when f_r shifts around f_m. For example, when ξ_i changes from 1.33 to 1.17 while keeping $f_i = 15.53$ GHz, f_r shifts from 30 to 27 GHz, shown as the

#261981 Received 28 Mar 2016; revised 23 Apr 2016; accepted 23 Apr 2016; published 27 Apr 2016

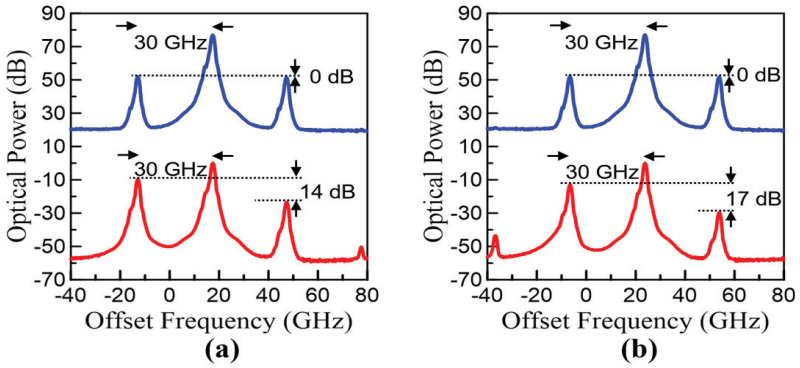

Fig. 6. Optical spectra of DSB inputs (blue curves) and SSB outputs (red curves) at $f_m =$ 30 GHz for (a) (ξ_i, f_i) = (1.17, 15.53 GHz) and (b) (ξ_i, f_i) = (1.33, 21.8 GHz), respectively. For visibility, the curves are up- or down-shifted with respect to each other. The x-axes are relative to the free-running frequency of LD2.

green curve in Fig. 3(a). Under this injection condition, an input DSB signal at $f_m = 30$ GHz can be converted to an output SSB signal with SRR = 14 dB, as Fig. 6(a) presents, of which SSB feature is close to the one demonstrated in Fig. 2(b) when $\xi_i = 1.33$. On the other hand, when f_i varies from 15.53 to 21.8 GHz while fixing $\xi_i = 1.33$, f_r shifts from 30 to 33 GHz, shown as the green curve in Fig. 3(b). As Fig. 6(b) presents, under this injection condition, an input DSB signal at $f_m = 30$ GHz can be converted to an output SSB signal with SRR = 17 dB, of which SSB feature is similar to the one demonstrated in Fig. 2(b) when $f_i = 15.53$ GHz. These results demonstrate that the system can stably operate under certain fluctuations of either ξ_i or f_i, which may result from possible fluctuations in the operating condition due to ambiance variations. As opposed to the period-one dynamics approach, no frequency locking between the modulation sidebands of an input DSB signal and the relaxation resonance sidebands of a stable locking dynamical state is necessary for the proposed approach to carry out the conversion when $f_r \neq f_m$. This characteristic makes the DSB-to-SSB conversion still feasible if ξ_i or f_i fluctuates considerably, i.e., if f_r is very far from f_m. For example, if SRR = 10 dB is the minimum requirement for an output SSB signal in a radio-over-fiber system to mitigate the microwave power fading effect to an acceptable level, the proposed conversion approach works well for $f_m = 30$ GHz even if ξ_i varies between 1.05 and 1.67 at $f_i = 15.53$ GHz or if f_i changes between 8.51 and 34.75 GHz at $\xi = 1.33$. The former and the latter correspond to a change of f_r between 25 and 35.6 GHz and between 26.6 and 40.9 GHz, respectively. This system stability under ξ_i or f_i variation ensures a functioning operation of the proposed conversion system over a significantly wide range of fluctuation in the input optical power and frequency.

3.4. Microwave stability and purity

Since the proposed conversion approach is mainly based on the nonlinear dynamical interaction that occurs inside the injected laser cavity, this raises concern of whether the stability and purity of the microwave subcarriers would deteriorate after conversion due to laser intrinsic noise. To investigate the microwave stability and purity, the 3-dB linewidth and the single-sideband phase noise, estimated as the ratio of the microwave power at a non-zero frequency offset to that at the zero, of the microwave subcarriers are analyzed. For the operating condition considered in Fig. 2(b) where $f_m = f_r$, the microwave linewidth after conversion is maintained below 1 Hz, as shown in Fig. 7(a), which is the highest resolution bandwidth of the microwave spectrum

#261981 Received 28 Mar 2016; revised 23 Apr 2016; accepted 23 Apr 2016; published 27 Apr 2016

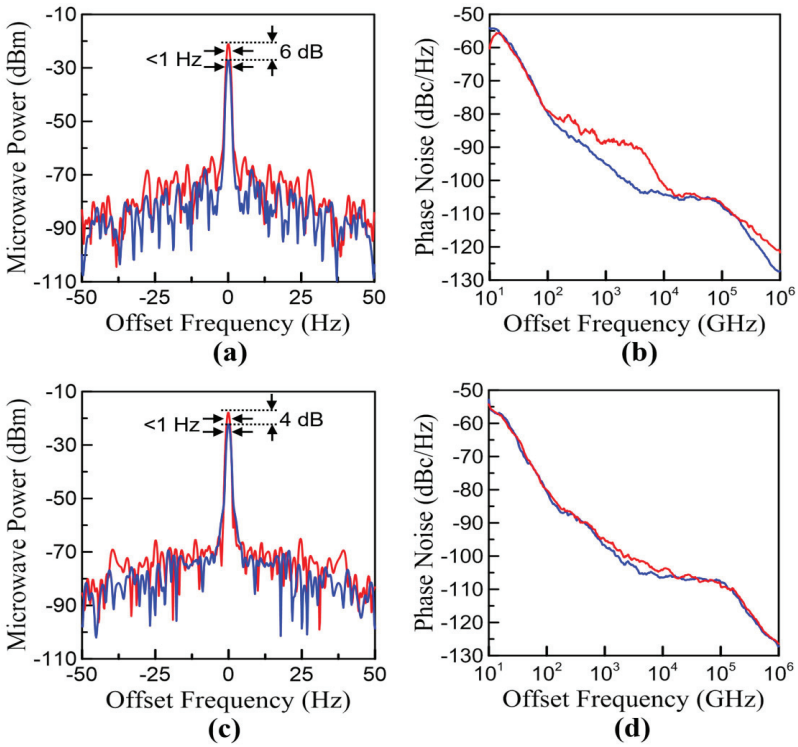

Fig. 7. (a) Microwave spectra, centering at 30 GHz, and (b) phase noise of the DSB input (blue curves) and the SSB output (red curves) at (ξ_i, f_i, f_m) = (1.33, 15.53 GHz, 30 GHz). (c) Microwave Spectra, centering at 25 GHz, and (d) phase noise of the DSB input (blue curves) and the SSB output (red curves) at (ξ_i, f_i, f_m) = (1.33, 15.53 GHz, 25 GHz). When measuring the microwave linewidth, the highest resolution of 1 Hz is used.

analyzer used in this study. In addition, the microwave phase noise of the output SSB signal follows closely with that of the input DSB signal over the frequency range under consideration, as shown in Fig. 7(b). These results suggest that the microwave stability and purity are mostly preserved after conversion.

Such preservation is as well observed not only for other operating conditions under study where $f_m = f_r$ but also for those where $f_m \neq f_r$. As an example, for the operating condition considered in Fig. 5(a) where $f_m \neq f_r$, the microwave linewidth and phase noise of the output SSB signal are highly similar to those of the input DSB signal, as Fig. 7(c) and 7(d) present, respectively. This result demonstrates that, even when f_m, ξ_i, or f_i fluctuates within a broad range, not only the proposed conversion system operates stably but also the microwave stability and purity are preserved after conversion.

3.5. Data quality

The preservation of the microwave stability and purity ensures that the quality of the data carried by the microwave subcarriers is maintained after conversion. Figure 8(a) presents the BER analysis at a data rate of 1.25 Gb/s for the operating condition considered in Fig. 2(b) where $f_m = f_r$. The BER behavior of the output SSB signal is similar to that of the input DSB signal, where a BER down to 10^{-9} is achieved. Their representative eye diagrams shown in Fig. 8(b) demonstrate not only clear and wide eye-opening but also similar time jitters. These results

#261981 Received 28 Mar 2016; revised 23 Apr 2016; accepted 23 Apr 2016; published 27 Apr 2016

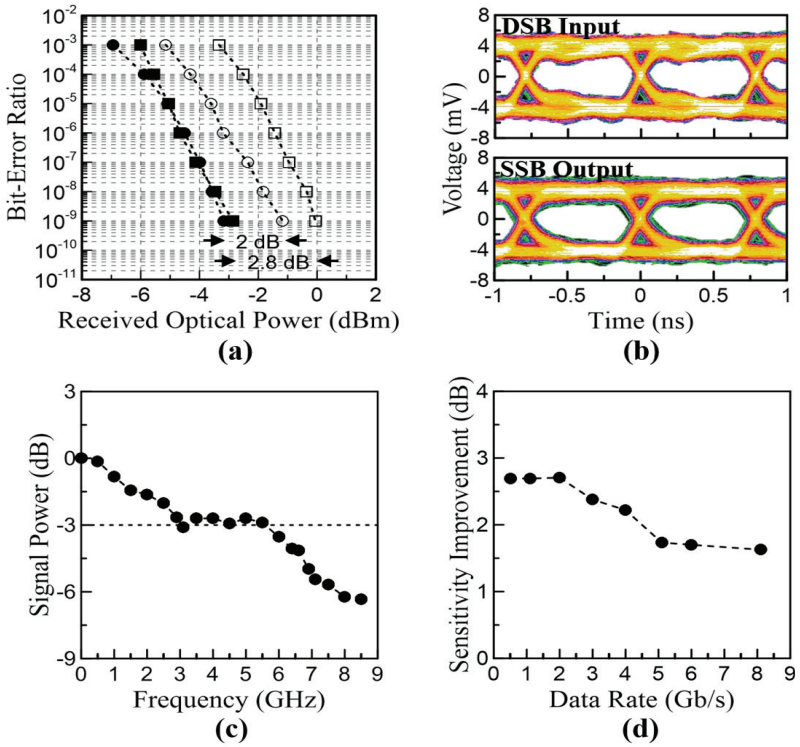

Fig. 8. (a) BER in terms of received optical power. Open and solid squares are results for the DSB input and the SSB output, respectively, at (ξ_i, f_i, f_m) = (1.33, 15.53 GHz, 30 GHz). Open and solid circles are results for the DSB input and the SSB output, respectively, at (ξ_i, f_i, f_m) = (1.33, 15.53 GHz, 25 GHz). All bit rates are fixed at 1.25 Gb/s with a bit sequence of $2^{31} - 1$. (b) Eye diagrams for the open and solid squares in (a), respectively, at BER = 10^{-9}. (c) Frequency response of the proposed system to modulation of the microwave subcarrier at (ξ_i, f_i, f_m) = (1.33, 15.53 GHz, 30 GHz). (d) Detection sensitivity improvement at BER = 10^{-9} in terms of data rate with a bit sequence of $2^9 - 1$ when (ξ_i, f_i, f_m) = (1.33, 15.53 GHz, 30 GHz).

suggest that the quality of the data is mostly preserved after conversion. Note that, except for the slight spectral broadening around both modulation sidebands, the extent of the SSB feature of the output optical signal shown in Fig. 2(b) is sustained even when a message is encoded onto the microwave subcarrier of the input DSB signal.

Figure 8(a) also shows an improvement of the detection sensitivity, about 2.8 dB, after conversion. Such an improvement results from the power amplification around the lower modulation sideband, in particular, of the output SSB signal because of the strong resonance enhancement around the lower relaxation resonance sideband of the injected laser. This can be verified by the result shown in Fig. 2(b), where the power of the lower modulation sideband is significantly enhanced by 13 dB after conversion. This gives rise to a considerable enhancement of the optical modulation depth of the output SSB signal, and therefore, as Fig. 7(a) presents, leads to power amplification of the microwave subcarrier, about 6 dB, after conversion. This result suggests that, through the same resonance enhancement mechanism, the data carried by the microwave subcarrier can also be amplified up to a similar level. Since the optical power received by the photodiode is proportional to the square root of the electrical power it gener-

#261981 Received 28 Mar 2016; revised 23 Apr 2016; accepted 23 Apr 2016; published 27 Apr 2016

ates, the improvement of the detection sensitivity shown in Fig. 8(a) is approximately half of the microwave amplification shown in Fig. 7(a).

Similar BER performance, eye diagrams, and detection sensitivity improvements are as well observed not only for other operating conditions under study where $f_m = f_r$ but also for those where $f_m \neq f_r$. As an example, for the operating condition considered in Fig. 5(a) where $f_m \neq f_r$, not only a BER down to 10^{-9} is achieved after conversion but also a detection sensitivity improvement of 2 dB is obtained, as Fig. 8(a) presents. This result demonstrates that, even when f_m, ξ_i, or f_i fluctuates within a broad range, not only the proposed conversion system operates stably but also the quality of the data carried by the input DSB signal is preserved after conversion.

For a data rate higher than 1.25 Gb/s, similar BER performance, eye diagrams, and detection sensitivity improvements can also be achieved. To investigate the highest possible data rate that the proposed conversion system can respond to, Fig. 8(c) demonstrates its frequency response to modulation of the input microwave subcarrier for the operating condition considered in Fig. 2(b). A 3-dB modulation bandwidth of about 5.5 GHz is observed, suggesting that the proposed conversion system can well respond to the modulation at a data rate up to at least 5.5 Gb/s. Note that the signal power shown in Fig. 8(c) is normalized with respect to the modulation of the input microwave subcarrier at each corresponding frequency in order to compensate for the different response of the Mach-Zehnder modulator used in this study at each frequency. Therefore, Fig. 8(c) also suggests the power amplification profile around the microwave subcarrier frequency through the resonance enhancement mechanism addressed above. Accordingly, to a certain extent, the 3-dB modulation bandwidth can also be used to indicate the gain bandwidth of the resonance enhancement provided by the proposed conversion system, suggesting that the detection sensitivity improvement can happen for a data rate up to more than 5.5 Gb/s. Figure 8(d) presents the dependence of the detection sensitivity improvement on the data rate under the operating condition considered in Fig. 2(b). A sensitivity improvement of more than 1.5 dB is observed up to 8 Gb/s, suggesting that the proposed conversion system responds well up to at least 8 Gb/s even though its 3-dB modulation bandwidth for the present operating condition is only about 5.5 GHz. Note that, owing to the bandwidth limitation of certain devices used in this study, only a data rate up to 8 Gb/s is demonstrated. If a detection sensitivity improvement of -3 dB, which is more commonly referred to as a 3-dB power penalty in the field of optical communications, is the minimum requirement for a radio-over-fiber system to maintain its quality of service, the proposed conversion system would also work well for a data rate much higher than 8 Gb/s based on Figs. 8(c) and 8(d).

3.6. Fiber distribution

To demonstrate the chromatic dispersion effect on the power of microwave subcarriers over fiber distribution, both input DSB signals and output SSB signals are sent through fibers of different lengths before photodetection. Figure 9(a) presents the power of the microwave subcarriers as a function of the fiber transmission distance for the operating condition considered in Fig. 2(b). To compensate for the optical power loss due to fiber attenuation, optical fiber amplifiers are used to ensure that the optical power received by the photodetector is the same for each data point under study. However, due to the limit of the available optical power, a total transmission distance of less than 40 km is investigated experimentally. Theoretical curves are also shown for comparison, which are calculated based on the following equation [5, 6]:

$$P_m \propto \left\{1 + S + 2\sqrt{S}\cos\left[2\pi c D l \left(\frac{f_m}{f_c}\right)^2\right]\right\} \quad (1)$$

#261981 Received 28 Mar 2016; revised 23 Apr 2016; accepted 23 Apr 2016; published 27 Apr 2016

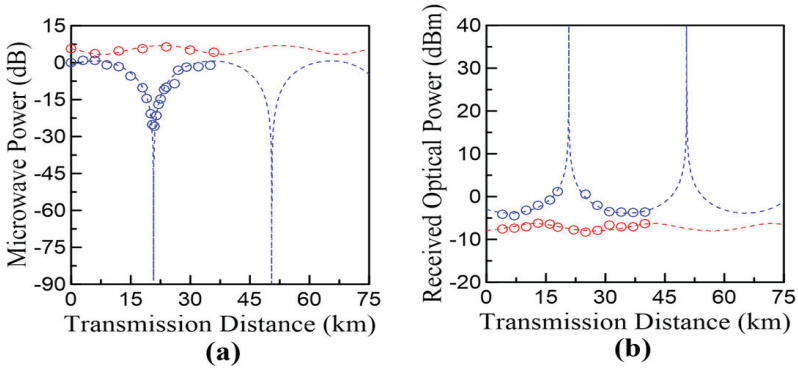

Fig. 9. (a) Microwave power and (b) received optical power as functions of fiber transmission distance for the input DSB signal (blue symbols and curves) and the output SSB signal (red symbols and curves) at (ξ_i, f_i, f_m) = (1.33, 15.53 GHz, 30 GHz).

where P_m is the microwave power of a microwave-modulated optical signal after photodetection, S is the sideband rejection ratio of the microwave-modulated optical signal and is defined as the relative strength of its lower modulation sideband to the upper one, c is the speed of light in free space, D is the dispersion coefficient at the optical carrier frequency f_c of the microwave-modulated optical signal, l is the fiber transmission distance, and f_m is the microwave frequency of the microwave-modulated optical signal. For the fibers used in this study, $D = 4.66$ ps/km-nm at $f_c = 193.426$ THz is adopted for the calculation shown in Fig. 9(a), and $S = 0$ and 14 dB are used for the input DSB signal and the output SSB signal, respectively, for the operating condition considered in Fig. 2(b). For the input DSB signal, a deep and repetitive variation of its microwave power is observed, resulting in a maximum power variation of about 27 dB under study. For the output SSB signal, by contrast, a significantly smaller power variation is experienced, leading to a maximum power variation of about 3 dB only. Note that the difference in the microwave power at 0 km between the input DSB signal and the output SSB signal reflects the fact that the microwave power is amplified after the DSB-to-SSB conversion based on the proposed approach.

The different behaviors of the microwave power as a function of the fiber transmission distance between the input DSB signal and the output SSB signal have significantly different impacts on their BER performances. Figure 9(b) presents the required level of the received optical power to achieve a BER of 10^{-3} as a function of the fiber transmission distance. BER $= 10^{-3}$ is chosen as a criterion here to meet the acceptable standard of BER $= 3.8 \times 10^{-3}$ with forward error correction in the field of optical communications. Theoretical curves are also presented for comparison, which are calculated based on Eq. (1) and the relation between the optical power received and the microwave power generated by a photodetector. For the input DSB signal, the received optical power required to achieve BER $= 10^{-3}$ enhances considerably around the transmission distance where the microwave power drops the most. It becomes more difficult to achieve error-free reception down to BER $= 10^{-3}$ if the transmission distance approaches more to the valley of the microwave power variation owing to the significantly weak microwave power. For the output SSB signal, by contrast, error-free reception is achieved over the fiber transmission distance under study with a maximum variation of only 2 dB in the received optical power required to achieve BER $= 10^{-3}$. Results similar to Figs. 7 to 9 are obtained no matter whether the DSB-to-SSB conversion is carried out before or after fiber distribution, which provides flexibility in the architecture design of a radio-over-fiber system.

#261981 Received 28 Mar 2016; revised 23 Apr 2016; accepted 23 Apr 2016; published 27 Apr 2016

4. Discussion and conclusion

Before concluding this study, a few remarks are made as follows to compare the stable locking dynamics approach demonstrated here with the period-one dynamics approach proposed in [13]. Different from the former, the latter requires frequency locking between the modulation sidebands of an input DSB signal and the oscillation sidebands of a period-one dynamical state in order to take advantage of the inherent power difference between the oscillation sidebands, typically more than 20 dB. Accordingly, as opposed to the stable locking dynamics approach, the DSB-to-SSB conversion is achieved with a higher SRR value, typically more than 20 dB, and a higher detection sensitivity improvement, up to at least 15 dB, using the period-one dynamics approach. However, the frequency-locking requirement limits the system adaptability and stability to a narrower range when operating conditions fluctuate and may also restrict the highest possible data rate to a lower value because of the narrower gain bandwidth. For example, if f_m deviates from f_r by 5 GHz as addressed in Sec. 3.3, the period-one dynamics approach cannot work unless a high enough optical modulation depth, such as 36% or higher, is used to achieve the required frequency locking.

In summary, an approach based on stable locking dynamics of a semiconductor laser is investigated for DSB-to-SSB conversion. By taking advantage of the significant difference in the resonance enhancement of the dynamics between negatively and positively offset frequencies from the laser oscillation, the conversion is achieved by considerably amplifying the lower modulation sideband of an input DSB signal as opposed to the upper one. The conversion can be achieved no matter how the input DSB signal is generated to begin with, such as external or direct modulation of a laser. Since the conversion relies solely on the nonlinear dynamical interaction between the input DSB signal and the laser, only a typical semiconductor laser is required as the key conversion unit, and no pump or probe signal is necessary. The conversion can be achieved for a broad tunable range of microwave subcarrier frequency up to at least 60 GHz by simply adjusting the frequency and power of the optical carrier of the input DSB signal relative to those of the laser. Since no frequency locking is required, the conversion can be achieved even when the operating condition fluctuates over a wide range owing to possible ambiance variations or different practical requirements, leading to high adaptability and stability of the conversion system. The phase quality, such as linewidth and phase noise, of microwave subcarriers is mainly preserved after conversion. Because of the wide bandwidth of the resonance enhancement, the rate of the data carried by the microwave subcarriers is high, up to at least 8 Gb/s. Similar results on the phase quality and data performance are obtained no matter whether the conversion is carried out before or after fiber distribution, providing flexibility in the architecture design of a radio-over-fiber system.

Acknowledgments

S.K. Hwang's work is supported by the Ministry of Science and Technology of Taiwan under Contract MOST103-2112-M-006-013-MY3 and Contract MOST104-2622-E-006-036-CC2, and also by the Asian Office of Aerospace Research and Development of the U.S. Air Force under Grant FA2386-14-1-0006 and Grant FA2386-15-1-4026. C.C. Lin's work is supported by the Ministry of Science and Technology of Taiwan under Contract MOST104-2218-E-011-014.

#261981 Received 28 Mar 2016; revised 23 Apr 2016; accepted 23 Apr 2016; published 27 Apr 2016